

1 Article

2 Monitoring the Damage of *Armyworm* as a Pest in 3 Summer Corn by Unmanned Aerial Vehicle Imaging

4 Wancheng Tao ^{1,2}, Xinsheng Wang ^{1,2}, Jing-Hao Xue ³, Wei Su ^{1,2*}, Mingzheng Zhang ^{1,2}, Dongqin
5 Yin^{1,2}, Dehai Zhu ^{1,2}, Zixuan Xie^{1,2}, Ying Zhang^{1,2}

6 ¹ College of Land Science and Technology, China Agricultural University, Beijing 100083, China

7 ² Key Laboratory of Remote Sensing for Agri-Hazards, Ministry of Agriculture, Beijing 100083, China

8 ³ Department of Statistical Science, University College London, London, WC1E 6BT, UK

9 * Correspondence: suwei@cau.edu.cn; Tel.: +86 010-6273-7855

10 Received: date; Accepted: date; Published: date

11 Abstract:

12 BACKGROUND: The timely, rapid, and accurate near real-time observations are urgent to monitor
13 the damage of corn *armyworm*, because the rapid expansion of *armyworm* would lead to severe yield
14 losses. Therefore, the potential of machine learning algorithms for identifying the *armyworm*
15 infected areas automatically and accurately by multispectral Unmanned Aerial Vehicle (UAV)
16 dataset is explored in this study. And the study area is in Beicuizhuang Village, Langfang City,
17 Hebei Province, which is the main corn-producing area in the North China Plain.

18 RESULTS: Firstly, we identified the optimal combination of image features by *Gini*-importance and
19 the comparison of four kinds of machine learning methods including Random Forest (RF),
20 Multilayer Perceptron (MLP), Naive Bayes Classifier (NB) and Support Vector Machine (SVM) was
21 done. And RF was proved to be the most potential with the highest *Kappa* and *OA* of 0.9709 and
22 0.9850, respectively. Secondly, the *armyworm* infected areas and healthy corn areas were predicted
23 by an optimized RF model in the UAV dataset, and the *armyworm* incidence levels were classified
24 subsequently. Thirdly, the relationship between the spectral characteristics of different bands and
25 pest incidence levels within the Sentinel-2 and UAV images were analyzed, and the B3 in UAV
26 images and the B6 in Sentinel-2 image were less sensitive for *armyworm* incidence levels. So the
27 Sentinel-2 image was used to monitor *armyworm* in two towns.

28 CONCLUSIONS: The optimized dataset and RF model are effective and reliable, which can be
29 used for identifying the corn damage by *armyworm* using UAV images accurately and
30 automatically in field-scale.

31 **Keywords:** *armyworm*; summer corn; Unmanned Aerial Vehicle; Random Forest; Sentinel-2
32

33 1. Introduction

34 The incidence of crop insect pests is increasing in China due to the frequent occurrence of
35 extreme weather and the increase of insect pests' resistance to insecticides in recent years¹. Curtis et
36 al. proven that crop pests will increase with global temperature. When average global surface
37 temperature increases by 2°C, corn production will be reduced by 23% in China and 32% in the
38 United States². *Armyworm* (*Mythimna separata* Walker) is one of the most serious insect pests on
39 cereal crops, resulting in great crop production loss every year³. Summer corn grows in hot rainy
40 season, as the high temperature and humidity create a perfect environment for *Armyworm* to
41 develop. The harm of *armyworm* to corn is huge, especially the second and third-generation larvae
42 with the characteristics of rapid outbreak⁴. In 2012, the *armyworm* broke out in most corn planted
43 areas of China, resulting in serious damage on corn production⁵.

44 The chemical pesticide is the primary method to control the *armyworm* presently. However,
45 over usage of pesticides will pollute the environment, and pesticide residues do harm to soil and
46 human health. Thus, it is of great significance to determine the occurrence area, severity and spread
47 pattern of *armyworm* pest rapidly and timely, for controlling the pest infestation by employing
48 precise spraying of pesticides in the field⁶. The traditional methods of monitoring *armyworm* are
49 mainly depended on the field campaign. It is time-consuming and laborious, and the field campaign
50 can be done only in finite sampling areas. Therefore, the laborious investigation method in the field
51 campaign cannot meet the requirements of timely and rational pesticide usage⁷. Therefore, many
52 studies explore the easy way to monitor the damage of *armyworm* pests. The *armyworm* mainly feeds
53 on the corn leaves and ears, especially in the tasseling-filling stage, which results in plant dwarfing
54 and corn canopy spectral signature changing. Considering these facts, remote sensing has emerged
55 as a promising way to identify crop diseases and insect pests non-destructively, quickly, and
56 automatically on a regional scale.

57 Many studies⁸⁻¹⁰ have revealed the effectiveness of satellite images in monitoring crop diseases
58 and insect pests. Unfortunately, the long revisit period, low spatial resolution, and the requirements
59 for clear weather of satellite images hampered monitoring the *armyworm* damage because the
60 *armyworm* would break out in a very short time¹¹. Recently, unmanned aerial vehicles (UAV) with
61 different carrying sensors act as a rapid and ongoing tool in precision agriculture. Many
62 researches¹²⁻¹⁴ have made lots of effort on crop monitoring by UAV images. With the advances in
63 flexible operation and high spatial, spectral, and temporal resolution, the UAV images can identify
64 the damaged plants and monitor damaged severity accurately¹⁵. Dobbels and Lorenz¹⁶ used a UAV
65 system to monitor soybean chlorosis caused by iron deficiency. They achieved better results than
66 traditional ground-based visual assessments. Yue et al.¹⁷ extracted pest information from UAV
67 images with an improved scale-invariant feature transform algorithm. Huang et al.¹⁸ explored the
68 potential using a photochemical reflectance index for quantifying the yellow rust in wheat from
69 airborne hyperspectral images. Due to the UAV can observe Stereo Image pairs, and the images can
70 be used to produce digital surface models (DSM) through photogrammetry using image-based
71 modeling (IBM) algorithm, which offers a cost-effective way to collect crop canopy structure
72 information¹⁹. As a co-product of UAV optical imaging, the DSM can be used to classify crop planted
73 area²⁰, monitor crop growth condition²¹, identify crop disasters, and estimate crop yield. However,
74 the potential of jointing the UAV spectral images, DSM features and spectral features to monitor the
75 *armyworm* infestation has few studies yet. Therefore, we search the optimal combination of the UAV
76 spectral images, DSM features and image features by *Gini*-importance for monitoring the damage of
77 *armyworm* for summer corn in this study.

78 Remote sensing data are massive and high-dimensional big data. Therefore, efficient and
79 automated approaches are critical to image analysis and interpretation²². The Random Forest (RF) is
80 one of the popular supervised classification methods with an ensemble learning algorithm, which
81 uses multiple decision trees to predict samplings²³. Moreover, RF can produce the importance of all
82 features in the classification, which helps reduce data dimension and improve efficiency²⁴.
83 Consequently, RF has been used in pest damage monitoring by UAV images. Adelabu et al.²⁵ used
84 RF and Support Vector Machine classification algorithms to identify different levels of insect
85 defoliation in an African savanna based on RapidEye imagery. Aparecido et al.²⁶ developed a
86 disease and pest warning system for coffee to predict the incidence of various diseases and insect
87 pests using the RF Regressor and Artificial Neural Networks. In summary, the pixel-based RF
88 method has attracted wide attention because it has good classification performance and processing
89 speed for crop disaster classification. Therefore, we use the RF to monitor the *armyworm* damage of
90 summer corn in this study based on the UAV dataset.

91 In this study, the RF algorithm is used to identify *armyworm* damage levels of summer corn by
92 pest incidence based on the UAV dataset. Moreover, the spectral characteristics of different pest
93 incidences in Sentinel-2 images are analyzed for exploring the potential of the satellite images. The
94 contributions of this paper lie in:

- 95 i) Identifying the important image features in the UAV dataset for identifying the *armyworm*
96 pests that occurred in corn planted areas.
- 97 ii) Exploring the potential of the RF model for monitoring the damage of *armyworm* pests of
98 summer corn, compared with three kinds of machine learning algorithms including MLP, NB and
99 SVM.
- 100 iii) Classifying the *armyworm* infected areas and healthy corn area by optimized RF model in
101 the UAV dataset. And the pest Levels are divided into five levels using Natural Breaks (Jenks) and
102 weighted average.
- 103 iv) Analyzing the relationship between the spectral characteristics of different bands and
104 different pest incidence levels in Sentinel-2 and UAV images. Combining UAV classification results
105 with Sentinel-2A images to monitor pest incidence levels in a large range.

106 2. Materials and Methods

107 2.1 Study area

108 The study area was located in Beicuizhuang Village, Langfang City, Hebei Province, China,
109 ranging from 116°44'E 39°21'N to 116°46'E 39°22'N, and covering an area of about 70 ha (Figure 1
110 (a)). This area was in the central-eastern part of the North China Plain. And there were various crops
111 were planted, including summer corn, soybean, peanut, apple trees, and other crops. This was a
112 typical small-holding farming area with irrigation by pumping water, and the crop management
113 (e.g., sowing, irrigation, fertilization and weeding) was varied. Conventionally, summer corn was
114 sowed at the end of June and harvested at the beginning of October in the study area. There were
115 some summer corn areas that were attacked seriously by *armyworm* in the middle of August 2019.

116 For monitoring the damage of *armyworm* pests, the UAV imaging and field campaign were done
117 simultaneously on 18 August, 2019. The collected UAV images (B2/ B3/ B1) and field data are shown
118 in Figure1 (b). According to the health condition of corn leaves, there were 24 representative field
119 plots that were collected for monitoring the damage of *armyworm* pests. And there were 5 samplings
120 in each plot which were distributed in the four corners and center of each plot. The size of each
121 sampling was 1m×1m. All measured samplings were located using Huace i80 real-time kinematic
122 (RTK) GPS receiver (Huace Ltd., Shanghai, China). The corn planted area in the study area could be
123 divided into two main groups through field campaign: (1) the summer corn planted area attacked by
124 *armyworm*, (2) the healthy summer corn planted area. In Figure1 (c), the left of each group was UAV
125 sub-images, and the right of each group was the field sample photos. Figure1 (c) showed that the
126 summer corn leaves attacked by *armyworm* are smaller and thinner, and the healthy corn planted
127 areas were more evenly distributed. Considering the significant influence of the sample quantity
128 and quality on model training, there were 1740 samples of healthy corn planted area, 1763 samples
129 of corn damaged area by *armyworm* were selected manually from UAV images according to the
130 measured data in field campaign and visual interpretation, and each sample is a pixel of UAV
131 image.

132 2.2 Image collection and feature dataset construction

133 2.2.1 UAV image collection

134 The UAV images were collected between 10:50 and 11:25 AM, 18 August 2019, when it was
135 sunny and windless. The Parrot Disco-Pro AG, a fixed-wing UAV system, was used to collect UAV
136 images. This system carried an automated multispectral sensor (Parrot Sequoia camera), which was
137 developed for agricultural applications. The multispectral bands include green, red, Red-edge and
138 near-infrared (NIR), and the spectral characteristics of the UAV image collected using the Parrot
139 Sequoia camera was shown in Table 1. The camera was connected to an irradiance sensor, which had
140 the same spectral bands as the multispectral sensor that could record the light conditions. In this
141 way, the image data was done radiometric calibration in real-time for illumination changing
142 automatically.

143 Before the flight, the image of the calibration board was captured by the Parrot Sequoia camera
 144 for radiation correction (Figure 2). It was noted that the calibration board must face the sun to make
 145 no shadows covering the radiation calibration board. Figure 2 (a) – (d) are the green, red, Red-edge,
 146 and NIR bands captured for radiometric calibration. The height of flight above ground was 120
 147 meters. The longitudinal overlap and side overlap were all 80%, with the ground sample distance
 148 (GSD) being 0.135 m/pixel. The georeferencing was achieved by Global Positioning System (GPS)
 149 built into the Parrot Sequoia camera and five ground control points (GCPs) were provided by using
 150 a Huace i80 real-time kinematic (RTK) GPS receiver (Huace Ltd., Shanghai, China) with 2.0 cm of
 151 positioning accuracy. The UAV photos, the calibration photos, and GCPs were input into the
 152 Pix4Dmapper Pro 4.1 software. The image splicing and point cloud modeling were done using “Ag
 153 Multispectral” template automatically²⁷. And the spliced multispectral image with $3,315 \times 5,176$
 154 (Figure 1(b)) was generated with a spatial resolution of 0.135 m/pixel.

155 2.2.2 Feature dataset construction

156 The Normalized Difference Vegetation Index (NDVI) is the most commonly used remote sensing
 157 vegetation index, which is calculated from the reflectance measurements in the near infrared
 158 (790 nm) and red (660 nm) portion of the spectrum in UAV images²⁸. The NDVI can be expressed by
 159 the following formula:

$$160 \quad \text{NDVI} = \frac{\rho_{\text{NIR}} - \rho_{\text{red}}}{\rho_{\text{NIR}} + \rho_{\text{red}}} \quad (1)$$

161 where, ρ_{NIR} and ρ_{red} are the NIR band and red band respectively. For the green crops, the
 162 reflectance of red band is small and the reflectance of NIR band is big. So the NDVI approaches 1
 163 when the crops are dense, and the NDVI approaches 0 when the crops are small. Therefore, NDVI
 164 is used to depict if the corn leaves are attacked by *armyworm*.

165 From the photos taken in the field campaign, it is observed that the leaves of the summer corn
 166 affected by *armyworm* are generally blade yellowing. The corn leaves waned by *armyworm* attack
 167 resulting in the low vegetation cover and spectral change. So, the Red-edge Normalized Vegetation
 168 Index (RENDVI) is calculated based on two bands including the red band and the Red-edge band.

$$169 \quad \text{RENDVI} = \frac{\rho_{\text{RE}} - \rho_{\text{red}}}{\rho_{\text{RE}} + \rho_{\text{red}}} \quad (2)$$

170 where, ρ_{RE} is the Red-edge band. Similar to the spectral index NDVI, RENDVI approaches 1 when
 171 the crops are dense and the NDVI approaches 0 when the crops are thin, which can be used to
 172 depict if the corn leaves are attacked by *armyworm*.

173 Considering the height of the corn affected by *armyworm* is generally lower, the corn canopy
 174 DSM is built up to depicting the canopy height difference between corn plants attacked by
 175 *armyworm* and the healthy corn plants. The corn canopy DSM is generated with the spatial
 176 resolution of 0.131 m by Pix4Dmapper Pro 4.1 software. Therefore, the features of the UAV image
 177 are composed of four spectral bands (green, Red, Red-edge, and NIR), DSM, and the spectral index
 178 features including NDVI and RENDVI.0

179 2.3 Machine learning classification methods for identifying corn pests areas

180 2.3.1 Multilayer Perceptron

181 The most important feature of multilayer perceptron (MLP) is that it has multiple neuron
 182 layers, so it is also called deep neural network. The first layer is the input layer, the last layer is the
 183 output layer, and the middle layer is the hidden layers. The optimal number of hidden layers and
 184 output neurons can be determined according to the specific application²⁹. Because this method has
 185 good generalization ability, it is popular in classifying the pest areas of planted corns.

186 2.3.2 Naive Bayesian

187 Naive Bayesian (NB) based on Bayesian theory is a widely used classification algorithm in
 188 machine learning and data mining, with the assumption that the variables predicted are the

189 Gaussian distributed and independent of each other. The classification is based on the conditional
 190 probability that each sample belongs to various classes³⁰. Compared with other methods, the NB
 191 method is applicable with few or no input parameters, which is uncomplicated and cost-effective in
 192 dealing with classification problems. In this study, the NB method is selected and used to identify
 193 the *armyworm* areas of planted corns.

194 2.3.3 Support vector machine

195 Support vector machine (SVM) classification via spatial features is a learning method based on
 196 statistical learning theory, which classifies the input sample features by solving the optimal
 197 hyperplane among many different classes³¹. The core of SVM is to solve the problem of dichotomy.
 198 For multi-classification problems, "one-to-many" classification method is usually adopted. For n
 199 classes, there are n hyperplanes that need to be solved. And there are n results will be produced
 200 after the prediction sample passes the discrimination of n optimal hyperplanes. And the optimal
 201 class will be produced finally. The SVM is a small sample learning method with good robustness,
 202 which is used to classify the pest areas of planted corns for the UAV dataset in this study.

203 2.3.4 Random Forest classification

204 Random forest classification algorithm is an integrated learning method based on the
 205 combination of multiple CART decision trees³². In order to divide the variable space completely,
 206 self-extraction of input samples and node random splitting techniques are used to construct multiple
 207 decision trees. The prediction results can be obtained through the majority voting strategy of the
 208 decision tree, and the error caused by a single parameter group can be avoided effectively. The RF
 209 can generate the importance of each dimension, which helps the feature selection and improve
 210 efficiency. Therefore, the RF algorithm can be adapted to classify the *armyworm* areas of planted
 211 corns for the UAV dataset.

212 2.4 Feature selection for classifying corn pests areas

213 The dimensions importance can be expressed with the *Gini*-importance³³ for high-dimensional
 214 UAV dataset. The *Gini* index is used to measure the impurity (degree of uncertainty) of the sampling
 215 set, which is the probability that a random sample is misclassified. The *Gini* impurity of the initial set
 216 is as the following formula:

$$217 \quad Gini(K) = \sum_{i=1}^n P(k_i) \times (1 - P(k_i)) \quad (3)$$

218 where, $K = \{k_i; i = 1, 2, 3, \dots, n\}$ is the collection of all classes, k_i is the classes i , n is total number of
 219 classes. The $P(k_i)$ is the probability of the k_i class. When the initial set is divided into multiple
 220 subsets, the *Gini* impurity is as the following formula:

$$221 \quad Gini_s = \sum_{j=1}^N P(x_j) \times Gini(x_j) \quad (4)$$

222 where, $x_j = \{j = 1, 2, 3, \dots, N\}$ is the j -th set in the initial set, N is the total number of subsets. $P(x_j)$ is the
 223 probability of x_j . $Gini_s$ is the *Gini* internal impurity of x_j , which is the *Gini*-importance and is used to
 224 calculate the contribution of each feature.

225 2.5 Accuracy assessment

226 There are two measurements used to assess the classification performance for the *armyworm*
 227 pest infested corn planted area, including the overall accuracy (OA) and Kappa coefficient. These
 228 measurements are calculated from a confusion matrix³⁴ of classification results. The confusion matrix
 229 includes TP (True Positive), FN (False Negative), FP (False Positive) and TN (Ture Negative). A
 230 5-fold cross-validation³⁵ is used to evaluate the accuracy of the classification. All the selected
 231 samplings are divided into 5 groups randomly, including 4 groups used for training and 1 group
 232 used for testing. The configurations of hardware used in this study are Intel(R) Core (TM) i7-8700
 233 CPU 3.20 GHz, 32 G RAM.

234 The OA indicates the proportion of correct pixels predicted, including pixels both healthy and
 235 attacked by insect pests. The OA can be as the following formula:

$$OA = \frac{TP+TN}{TP+FN+FP+TN} \quad (5)$$

where, TP and FN are the numbers of correct and wrong classifications of samples in the healthy corn category; FP and TN are the number of wrong and correct classifications of samples in the *armyworm* pest category.

The *Kappa* coefficient is a statistical indicator of interrater reliability, which is calculated by the *OA* and the probability of random agreement. The *Kappa* coefficient can be as the following formula,

$$Kappa = \frac{OA-P_e}{1-P_e} \quad (6)$$

where, P_e is the probability of random agreement. The *Kappa* is an index to measure the spatial consistency of classification results, which reveals the spatial changes of classification results clearly.

Then the P_e is as the following formula:

$$P_e = \frac{(TP+FN) \times (TP+FP) + (FP+FN) \times (FN+TN)}{TP+FN+FP+TN} \quad (7)$$

3. Results and Analysis

3.1 Optimize UAV dataset by *Gini*-importance and Random Forest method

The RF method is used to classify the summer corn planted area infested by *armyworm* for the UAV dataset. The zoomed sub-plots of the UAV dataset including pest infested area and healthy area are as shown in Figure 3. Figure 3 (a1) - (g1) are the image features of *armyworm* pest infested corn planted area, (a2) - (g2) are the features images of healthy corn planted area with the image features of green band, red band, red-edge band, NIR band, DSM, NDVI and RENDVI, respectively. From Figure 3(a1) - (g1), it can be seen that the tone difference is obvious and the image features are more heterogenous and blurry for *armyworm* infested areas than healthy area, especially in (a1), (b1), (f1) and (g1). Comparatively, the tone difference is relatively small and homogeneity exists in healthy corn planted areas in Figure 3 (a2) - (g2).

In order to determine the importance of each image feature in the UAV dataset, *Gini*-importance (Eq. 4) is used to measure and calculate the importance of image features in this study. Moreover, the parameters of RF are default, and the importance and the evaluation measures take the mean value of ten times experiment. The importance order of the UAV dataset image features for the identification of *armyworm* infested area is that NDVI (0.2933) > RENDVI (0.2061) > B2-Red (0.1677) > B4-NIR (0.1461) > DSM (0.0885) > B1-Green (0.0672) > B3-Red-edge (0.0308), as shown in Figure 4. And Figure 4 revealed that the importance of all features is greater than 0.03 and the top three important features for the classification model are the NDVI, RENDVI and B2-Red. It is clear that the vegetation index features (NDVI and RENDVI) bring the greatest contribution to classification.

With the same training samples, different features combinations are used to identify *armyworm* infested areas. The features in the UAV dataset are sorted by importance and the construction of each model in line with the importance of all features, and the performance of models is compared using the accuracy for selecting the optimal feature combination. The *Kappa* and *OA* are used to evaluate the performance of the different models quantitatively. And the experimental results are shown in Table 2. According to Table 2, the Model7 with all the features has the best quantitative evaluation results with *Kappa* and *OA* are 0.9709 and 0.9850, respectively. Compared to Model1 with a single image feature (RENDVI) only, the Model2, Model3, Model4, Model5, Model6 and Model 7 improved 0.1860/0.0906, 0.1933/0.0993, 0.1925/0.0990, 0.2019/0.1037, 0.2072/0.1064 and 0.2098/0.1078 in *Kappa* and *OA*, respectively. We also found that the model performance is constantly improved with the increase of features numbers. Compared with Model8 which only uses four features (Green, Red, Red-edge and NIR) and Model9 which uses five features (Green, Red, Red-edge, NIR and DSM), the Model7 improved 0.0301/0.0209 and 0.0195/0.0115 in *Kappa/OA*. This revealed that the joint of the DSM, NDVI and RENDVI could improve the performance of the classifier effectively. It is further proof that the features of the designed dataset in this study are reasonable and effective.

283 3.2 Comparison of performance for different machine learning algorithms

284 The performance of different machine learning methods is compared to verify the superiority of
 285 the RF. And there are three machine learning methods including MLP, NB and SVM are compared
 286 with RF. For all the methods in these experiments, this comparison is done using the same
 287 cross-validation method and the evaluation measures, which are 5-fold cross-validation and
 288 *Kappa/OA*, respectively. In addition, all training and testing datasets of the RF experiments (Model7)
 289 are used to the other three classification (MLP, NB and SVM) experiments for ensuring a fair
 290 comparison. The good model parameters of MLP, NB and SVM are selected according to experience,
 291 and the parameters of RF are default. For MLP classification method²⁹, the initial learning the
 292 activation functions are 0.001 and “RELU”, there are 2 hidden layers with 100 neurons per hidden
 293 layer. For NB classification method³⁰, there is only one major parameter, the prior probability, which
 294 is set as default without giving the prior probability. For SVM classification method³¹, the main
 295 parameters are as follows: the kernel type is radial basis function, gamma value is “auto” in the
 296 kernel function, and cost or slack parameter is 1.0. The quantitative evaluation results for different
 297 machine learning methods are shown in Table 3.

298 According to Table 3, the classification performance of four machine learning methods is
 299 greater than 0.91/0.95 (*Kappa/OA*). Compared with MLP, NB and SVM, the RF method improved
 300 0.0513, 0.0308 and 0.0285 in *Kappa*, and improved 0.0258, 0.0213 and 0.0205 in *OA*, respectively. It
 301 revealed that the RF classifier had the highest accuracy in distinguishing healthy and *armyworm*
 302 pests on corn. At the same time, the superiority of the RF classifier is also proved.

303 3.3 Mapping of *armyworm* infested area

304 Based on the comparison of the performance of different methods, the RF method is more
 305 applicable to mapping *armyworm* areas. The parameters of the RF method (Model7) can be
 306 optimized by random search and grid search furtherly. Firstly, the random searching method is used
 307 to estimate roughly the range of parameters, the number of decision trees is (80, 100), the maximum
 308 depth of decision trees is (90, 120). Secondly, the grid search method is used to optimize the
 309 parameters furtherly, the search step is 1. Finally, the optimal combination of parameters is obtained,
 310 the number of decision trees is 91, the maximum depth of decision trees is 107. The *Kappa* and *OA*
 311 of retrained RF (Model 7) are 0.9735 and 0.9864 based on optimized parameters. The mapping of
 312 *armyworm* infested areas is done using optimized RF (Model 7) subsequently, and the results as
 313 shown in Figure 5.

314 According to Figure 5, the pink areas are *armyworm* infested areas, and the green areas are
 315 healthy corn planted areas. A, B, C and D are the measured field plots in field campaigns where
 316 *armyworm* occurs seriously. The *armyworm* infestation occurs in the southwest of field plot A, the
 317 top center of field plot B, and nearly the whole of field plot C and D mainly. In addition, the
 318 reliability of the classification results is verified by field survey points. Four representative field
 319 survey photos are shown at four measured points from (p1) to (p4). The (p1) and (p2) are located in
 320 plots A and B, which are in the area with serious *armyworm* pests. It can be seen from the photos that
 321 most of the corn leaves are affected by *armyworm*, and the leaves are relatively few and small,
 322 resulting in the serious changes in corn canopy and morphology. On the other hand, (p3) and (p4)
 323 are in the healthy area, which is consistent with the obtained field survey photos.

324 3.4 Mapping of pest incidence level

325 To determine the severity of *armyworm* pests, and give some hints for pesticide spraying, the
 326 pest incidence level mapping is done. The NDVI can describe the vegetation growing condition,
 327 and the *Gini*-importance of NDVI features in Section 3.1 is the most prominent to UAV image
 328 classification. Natural Breaks (Jenks) method can best group similar values and maximize the
 329 differences between classes³⁶, which is a good method for grade classification. According to corn
 330 damage scales³⁷, the *armyworm* pest areas (the pink areas) in Figure 5 are divided into four levels
 331 based on NDVI value using Natural Breaks (Jenks). The levels include Level 1($0.23 \leq \text{NDVI} \leq 0.522$,

332 little damage), Level 2($0.12 \leq \text{NDVI} < 0.23$, medium damage), Level 3($0.01 \leq \text{NDVI} < 0.12$, heavy
 333 damage) and Level 4($-0.22 \leq \text{NDVI} < 0.01$, very heavy damage), and healthy corn is Level 0(No
 334 damage). The result of pest incidence levels is shown in Figure 6(a), the green area is Level 0, and
 335 the red area indicates the most serious pest incidence (Level 4).

336 Infesting levels of insect pests can be extended to $10\text{m} \times 10\text{m}$ grid. First, assign values 0, 1, 2, 3,
 337 and 4 to Level 0, Level 1, Level 2, Level 3, and Level 4 in Figure 6(a). Then, the mean value of pixels
 338 in $10\text{m} \times 10\text{m}$ grid is calculated as the grid value. The method Natural Breaks (Jenks) is used to
 339 classify damaged corn of the grids. The levels include Level 0[0, 0.172), Level 1[0.172, 0.58), Level
 340 2[0.58, 1.21), Level 3[1.21, 2.04) and Level 4[2.04, 4]. The result of pest levels based on grids is shown
 341 in Figure 6(b).

342 It can be found that the red areas are the largest in A, B, C and D field plots, indicating the
 343 highest pest levels, which is consistent with field observations and Figure 5. In terms of pest level,
 344 plots A and B, C and D are adjacent to each other, and the infested areas are connected. In the early
 345 stage of the pest incidence, the farmers in field plots A, B, C, and D did not find out the *armyworm*
 346 infection timely and did not take appropriate management for preventing the pest from spreading.
 347 This could be the reason for the local *armyworm* outbreak in the cornfield. Furthermore, we also
 348 found that the height of weeds is higher than the corn plants in damaged corn plots, and result in a
 349 humid and airless environment, which might also be one of the important reasons for the outbreak
 350 of *armyworm*.

351 3.5 Spectral reasoning for mapping of pest incidence level

352 The Sentinel-2 image³⁸ has more abundant spectral information than the UAV image, which is
 353 likely to be beneficial for pest monitoring. The spectral characteristics of different pest levels are
 354 analyzed for the Sentinel-2 image and the UAV images. For unifying the analyzing unit of spectral
 355 difference, the obtained Sentinel-2 image on 18 August 2019 in the study area is reconstructed with
 356 super resolution using SupReME³⁹, and each band is unified to 10m spatial resolution. After that,
 357 the spectral characteristics of Sentinel-2 image before and after super resolution reconstruction are
 358 analyzed, mainly in the building and corn planted area, which is as shown in Figure 7. In Figure 7,
 359 the orange line (predictive value) is the reflectance spectral curve after SupReME reconstruction, the
 360 red line (truth value) is the reflectance spectral curve of Sentinel -2. Figure 7 (a) is the spectral
 361 contrast of corn planted area, (b) is spectral contrast of buildings, the RMSE (Root Mean Square
 362 Error) are 0.00169 (a) and 0.008085 (b), respectively. The RMSE is close to zero, and the spectrum is
 363 basically unchanged.

364 The Sentinel-2 image with 10m spatial resolution and UAV images with a resolution of 0.135m
 365 are used to analyze the spectral characteristics of different pest levels. There are 600 sampling
 366 points and 250 sampling points are selected based on Figure 6(a) and Figure 6(b) respectively to
 367 calculate the mean values of each band of UAV and Sentinel-2 images. The statistical results as
 368 shown in Figure 8. The X-axis are band numbers and the Y-axis is spectral reflectance, different
 369 colors indicate different levels of pests. In Figure 8(a), with the pest level declines, the spectral
 370 reflectance of B1, B2, B3, B4, B5, B11 and B12 decreases, the spectral reflectance of B7, B8 and B8A
 371 increases. The spectral reflectance of B9 can distinguish between healthy and unhealthy corn areas,
 372 B6 is not clear. In Figure 8(b), B1 and B2 reveal that the spectral reflectance decreases with the pest
 373 level declines. B4 can distinguish between healthy corn and damaged corn. B3 is similar to B6 in the
 374 Sentinel-2 image, the relationship between reflectivity and pest level is not very clear. Sentinel-2
 375 and UAV images have similar characteristics in different pest levels in corresponding wavelength
 376 bands.

377 4. Discussions

378 The corn area damaged by *armyworm* resulted in the changing of corn canopy spectral
 379 reflectance since the changed morphological and chemical characteristics of leaves⁴⁰. In Figure 8(b),
 380 the bands involved in the vegetation index calculation are sensitive to the *armyworm* pest infestation,
 381 the NDVI and RENDVI features bring the greatest contribution to the classification. The height of

382 corn plants infested by *armyworm* is lower than healthy plants, which brings the DSM is also
 383 sensitive to the pest infestation of summer corn. It shows that the addition of vegetation index and
 384 DSM is beneficial to accurate classification.

385 As is known, the red-edge band (B5, B6 and B7 of Sentinel-2 and B3 of UAV) was one of the
 386 most sensitive bands to vegetation diseases⁴¹. In Figure 8 (a), with the change of corn *armyworm*
 387 incidence levels, the spectral characteristics of the red-edge bands change as well. With the decrease
 388 of corn *armyworm* incidence, the reflectance of B5 decreases, and the reflectance of B7 increases. The
 389 B6 of Sentinel-2 and the B3 of UAV are between B5 and B7, and the spectral intervals were only
 390 about 40 nm, which makes the sensitivity of the band (B6 of Sentinel-2 or the B3 of UAV) to the pest
 391 change lower than other bands⁴². B1, B2, B3 and B4 of Sentinel-2 and the B1 and B2 of UAV were the
 392 visible spectrum band where the leaves could rely on various pigments (i.e., chlorophyll,
 393 carotenoids) to absorb this energy. with corn canopy pigment decrease, visible light absorption
 394 decreases, which resulted in the increase of visible reflectance. B7, B8, B8A and B9 of Sentinel-2 and
 395 the B4 of UAV were the near-infrared bands and were related closely to the cell structure. The
 396 canopy reflectance was lower than healthy corn, indicating that the *armyworm* had seriously
 397 damaged the cell structure of the corn. Moreover, B11 and B12 were related to the water content of
 398 vegetation. In the area damaged by *armyworm*, the leaves of the plants gradually withered and the
 399 water content decreased, which led to the increase in spectral reflectance compared with normal
 400 vegetation.

401 The result of Figure 7 and Figure 8 revealed the performance of abundant spectral information
 402 of Sentinel-2 image had a great advantage in monitoring the damage of *armyworm* in the regional
 403 area. The Towns (An ci) in the UAV flight area and adjacent towns (Yong qing) are used as
 404 experimental areas (Figure 9(a)), the obtained Sentinel-2 images (18 August 2019) after SupReME
 405 reconstruction were attempted to classify pest levels. There are selected 250 sampling points based
 406 on Figure 6(b), and the training dataset and test dataset are divided into 7:3 for the RF model. The
 407 classification results as shown in Figure 9(b), the *OA* of train and validation are 0.76 and 0.69.
 408 Different colors correspond to different pest levels, the 'Level 5' in legend was the non-corn area.
 409 The non-corn area was obtained by Google Earth Engine platform classification using RF based on
 410 Sentinel-2 image (18 August 2019), which overall validation accuracy is 0.92. Figure 9(c) is the
 411 sub-image of Figure 9 (b), and the black box is the UAV flight area. The UAV flight area in Figure
 412 9(c) was consistent with the classification results (Figure 6(b)) of UAV basically, which revealed the
 413 effectiveness of classifying *armyworm* levels based on Sentinel-2 images. The areas of Level 3 and
 414 Level 4 were very small and the proportion of insect pest areas was low, indicating that the planted
 415 corns were generally healthy. The damaged levels by *armyworm* are classified from Sentinel-2
 416 images, which could provide data support for pesticide spraying and pest prevention in a large
 417 area.

418 5. Conclusions

419 The *armyworm* is one of the most serious insect pests of corn. We proposed a method to
 420 monitor the damaged scale by pest in summer corn based on UAV images. The conclusions can be
 421 drawn as follows.

422 (1) The importance of image features in the UAV dataset is determined by *Gini*-importance.
 423 The importance of images features is sorted as NDVI (0.2933) > RENDVI (0.2061) > B2-Red (0.1677) >
 424 B4-NIR (0.1461) > DSM (0.0885) > B1-Green (0.0672) > B3-Red-edge (0.0308). The NDVI is the most
 425 sensitive, while the B3 of UAV has the lowest sensitivity to *armyworm* pests.

426 (2) The RF model has the best performance for the classification of the *armyworm* pest and
 427 healthy corn compared to different machine learning methods (MLP, NB and SVM). The
 428 parameters of the RF can be optimized by random search and grid search furtherly, which are used
 429 to retrain the model. The classification results of the UAV dataset are predicted subsequently.

430 (3) The spectral characteristics of sentinel-2 and UAV images with different pest levels are
 431 analyzed. With the pest level declines, the spectral reflectance of B1 and B2 decreases, B3 is not very
 432 clear, B4 can distinguish healthy corn and damaged corn in UAV images. With the pest level

433 increases, the spectral reflectance of B1-B5 and B11-B12 increased, B7, B8 and B8A decreased, B6
 434 and B9 have no clear characteristics in the Sentinel-2 image. Furthermore, the classification of pest
 435 levels based on Sentinel-2 image using the RF model has achieved good results.

436 Due to the small geographical coverage of UAV images, the experimental area is small and
 437 restricted relatively. In the future, we will expand the research to explore the *armyworm* infestation
 438 of other similar crops (e.g., wheat and rice) and monitor the damage of pests on a larger scale. Then,
 439 coupling the crop growth models (e.g., WOFOST, DSSAT) or radiation transfer models (e.g.,
 440 PROSAIL, DART) with machine learning techniques will be tried, which maybe have potential in
 441 estimating the damage of *armyworm* pests. Furthermore, the multi-temporal UAV images and
 442 satellite images can be combined tentatively to detect insect pests in the field dynamically, which can
 443 support more informed farming decisions.
 444

445 **Author Contributions:** This work was a cooperation of our research team, and the contributions were as
 446 follows: Conceptualization, Mingzheng Zhang, Jing-Hao Xue and Wei Su; Formal analysis and Writing –
 447 review & editing, Jing-Hao Xue and Dongqin Yin; Investigation, Xincheng Wang, Wei Su and Dehai Zhu;
 448 Methodology and Writing – original draft, Mingzheng Zhang; Software, Mingzheng Zhang and Wancheng Tao;
 449 Validation, Zixuan Xie.

450 **Funding** This study was funded by the National Natural Science Foundation of China under the projects (No.
 451 42171331), the 2115 Talent development Program of China Agricultural University.

452 **Availability of data and materials**

453 The datasets used and/or analyzed during the current study available from the corresponding author on
 454 reasonable request.

455 **Acknowledgments:** We thank the farmers for allowing us to measure their fields.

456 **Competing interests:**

457 The authors declare that they have no competing interests.
 458

459 **References**

- 460 1. Xu HX, Yang YJ, Lu YH, Zheng XS, Tian JC, Lai FX, et al., Sustainable Management of Rice Insect Pests
 461 by Non-Chemical-Insecticide Technologies in China. *Rice Sci* **24**: 61-72 (2017).
- 462 2. Deutsch CA, Tewksbury JJ, Tigchelaar M, Battisti DS, Merrill SC, Huey RB, et al., Increase in crop
 463 losses to insect pests in a warming climate. *Science* **361**: 916-919 (2018).
- 464 3. Yasoob H, Abbas N, Li YF and Zhang YL, Selection for resistance, life history traits and the
 465 biochemical mechanism of resistance to thiamethoxam in the maize armyworm, *Mythimna separata*
 466 (Lepidoptera: Noctuidae). *Phytoparasitica* **46**: 627-634 (2018).
- 467 4. Serbesoff-King K, Melaleuca in Florida: A literature review on the taxonomy, distribution, biology,
 468 ecology, economic importance and control measures. *J Aquat Plant Manage* **41**: 98-112 (2003).
- 469 5. Liu J and Jiang Y, Characteristic of Corn Diseases and Pest in 2012 and Cause Analysis. *Chinese*
 470 *Agricultural Science Bulletin* **30**: 270-279 (2014).
- 471 6. Godfray HCJ, Beddington JR, Crute IR, Haddad L, Lawrence D, Muir JF, et al., Food Security: The
 472 Challenge of Feeding 9 Billion People. *Science* **327**: 812-818 (2010).
- 473 7. Klausner D, Challenges in monitoring and managing plant diseases in developing countries. *J Plant Dis*
 474 *Protect* **125**: 235-237 (2018).
- 475 8. Yuan L, Bao ZY, Zhang HB, Zhang YT and Liang X, Habitat monitoring to evaluate crop disease and
 476 pest distributions based on multi-source satellite remote sensing imagery. *Optik* **145**: 66-73 (2017).

- 477 9. Chemura A, Mutanga O and Dube T, Separability of coffee leaf rust infection levels with machine
478 learning methods at Sentinel-2 MSI spectral resolutions. *Precis Agric* **18**: 859-881 (2017).
- 479 10. Meigs GW, Kennedy RE, Gray AN and Gregory MJ, Spatiotemporal dynamics of recent mountain pine
480 beetle and western spruce budworm outbreaks across the Pacific Northwest Region, USA. *Forest Ecol*
481 *Manag* **339**: 71-86 (2015).
- 482 11. Eklundh L, Johansson T and Solberg S, Mapping insect defoliation in Scots pine with MODIS
483 time-series data. *Remote Sens Environ* **113**: 1566-1573 (2009).
- 484 12. Su W, Zhang MZ, Bian DH, Liu Z, Huang JX, Wang W, et al., Phenotyping of Corn Plants Using
485 Unmanned Aerial Vehicle (UAV) Images. *Remote Sens-Basel* **11**(2019).
- 486 13. Li X, Giles DK, Andaloro JT, Long R, Lang EB, Watson LJ, et al., Comparison of UAV and fixed-wing
487 aerial application for alfalfa insect pest control: evaluating efficacy, residues, and spray quality. **n/a**.
- 488 14. Roosjen PP, Kellenberger B, Kooistra L, Green DR and Fahrentrapp J, Deep learning for automated
489 detection of *Drosophila suzukii*: potential for UAV-based monitoring. **76**: 2994-3002 (2020).
- 490 15. Zarco-Tejada PJ, Gonzalez-Dugo V and Berni JAJ, Fluorescence, temperature and narrow-band indices
491 acquired from a UAV platform for water stress detection using a micro-hyperspectral imager and a
492 thermal camera. *Remote Sens Environ* **117**: 322-337 (2012).
- 493 16. Dobbels AA and Lorenz AJ, Soybean iron deficiency chlorosis high throughput phenotyping using an
494 unmanned aircraft system (vol 15, 97, 2019). *Plant Methods* **15**(2019).
- 495 17. Yue JW, Lei TJ, Li CC and Zhu JQ, The Application of Unmanned Aerial Vehicle Remote Sensing in
496 Quickly Monitoring Crop Pests. *Intell Autom Soft Co* **18**: 1043-1052 (2012).
- 497 18. Huang W, Lamb DW, Niu Z, Zhang Y, Liu L and Wang J, Identification of yellow rust in wheat using
498 in-situ spectral reflectance measurements and airborne hyperspectral imaging. *Precis Agric* **8**: 187-197
499 (2007).
- 500 19. Zarco-Tejada PJ, Diaz-Varela R, Angileri V and Loudjani P, Tree height quantification using very high
501 resolution imagery acquired from an unmanned aerial vehicle (UAV) and automatic 3D
502 photo-reconstruction methods. *Eur J Agron* **55**: 89-99 (2014).
- 503 20. Diaz-Varela RA, Zarco-Tejada PJ, Angileri V and Loudjani P, Automatic identification of agricultural
504 terraces through object-oriented analysis of very high resolution DSMs and multispectral imagery
505 obtained from an unmanned aerial vehicle. *J Environ Manage* **134**: 117-126 (2014).
- 506 21. Yang MD, Huang KS, Kuo YH, Tsai HP and Lin LM, Spatial and Spectral Hybrid Image Classification
507 for Rice Lodging Assessment through UAV Imagery. *Remote Sens-Basel* **9**(2017).
- 508 22. Troya-Galvis A, Gancarski P and Berti-Equille L, Remote sensing image analysis by aggregation of
509 segmentation-classification collaborative agents. *Pattern Recogn* **73**: 259-274 (2018).
- 510 23. Svetnik V, Liaw A, Tong C, Culberson JC, Sheridan RP and Feuston BP, Random forest: A
511 classification and regression tool for compound classification and QSAR modeling. *J Chem Inf Comp Sci*
512 **43**: 1947-1958 (2003).
- 513 24. Belgiu M and Dragut L, Random forest in remote sensing: A review of applications and future
514 directions. *Isprs J Photogramm* **114**: 24-31 (2016).
- 515 25. Adelabu S, Mutanga O and Adam E, Evaluating the impact of red-edge band from Rapideye image for
516 classifying insect defoliation levels. *Isprs J Photogramm* **95**: 34-41 (2014).
- 517 26. Aparecido LED, Rolim GD, De Moraes JRDC, Costa CTS and de Souza PS, Machine learning
518 algorithms for forecasting the incidence of *Coffea arabica* pests and diseases. *Int J Biometeorol* **64**:
519 671-688 (2020).

- 520 27. Fernandez-Guisuraga JM, Sanz-Ablanedo E, Suarez-Seoane S and Calvo L, Using Unmanned Aerial
521 Vehicles in Postfire Vegetation Survey Campaigns through Large and Heterogeneous Areas:
522 Opportunities and Challenges. *Sensors-Basel* 18(2018).
- 523 28. Hassan MA, Yang MJ, Rasheed A, Yang GJ, Reynolds M, Xia XC, et al., A rapid monitoring of NDVI
524 across the wheat growth cycle for grain yield prediction using a multi-spectral UAV platform. *Plant Sci*
525 282: 95-103 (2019).
- 526 29. Zhao CH, Gao YS, He J and Lian J, Recognition of driving postures by multiwavelet transform and
527 multilayer perceptron classifier. *Eng Appl Artif Intel* 25: 1677-1686 (2012).
- 528 30. Wang Q, Garrity GM, Tiedje JM and Cole JR, Naive Bayesian classifier for rapid assignment of rRNA
529 sequences into the new bacterial taxonomy. *Appl Environ Microb* 73: 5261-5267 (2007).
- 530 31. Koda S, Zeggada A, Melgani F and Nishii R, Spatial and Structured SVM for Multilabel Image
531 Classification. *Ieee Transactions on Geoscience and Remote Sensing* 56: 5948-5960 (2018).
- 532 32. Zhang J, Huang Y, Reddy KN and Wang BJPMS, Assessing crop damage from dicamba on non-
533 dicamba-tolerant soybean by hyperspectral imaging through machine learning. 75: 3260-3272 (2019).
- 534 33. Menze BH, Kelm BM, Masuch R, Himmelreich U, Bachert P, Petrich W, et al., A comparison of random
535 forest and its Gini importance with standard chemometric methods for the feature selection and
536 classification of spectral data. *Bmc Bioinformatics* 10(2009).
- 537 34. Goutte C and Gaussier E, A probabilistic interpretation of precision, recall and F-score, with
538 implication for evaluation. *Advances in Information Retrieval* 3408: 345-359 (2005).
- 539 35. Rodriguez JD, Perez A and Lozano JA, Sensitivity Analysis of k-Fold Cross Validation in Prediction
540 Error Estimation. *Ieee T Pattern Anal* 32: 569-575 (2010).
- 541 36. Chen J, Yang S, Li H, Zhang B and Lv JJIAPRSSIS, Research on geographical environment unit division
542 based on the method of natural breaks (Jenks). 3: 47-50 (2013).
- 543 37. Toepfer S, Fallet P, Kajuga J, Bazagwira D, Mukundwa IP, Szalai M, et al., Streamlining leaf damage
544 rating scales for the fall armyworm on maize. *J Pest Sci* 94: 1075-1089 (2021).
- 545 38. Sims NC, De Barro P, Newnham GJ, Kalyebi A, Macfadyen S and Malthus TJJPms, Spectral
546 separability and mapping potential of cassava leaf damage symptoms caused by whiteflies (*Bemisia*
547 *tabaci*). 74: 246-255 (2018).
- 548 39. Zhang M, Su W, Fu Y, Zhu D, Xue J-H, Huang J, et al., Super-resolution enhancement of Sentinel-2
549 image for retrieving LAI and chlorophyll content of summer corn. 111: 125938 (2019).
- 550 40. Gilioli G, Schrader G, Baker RHA, Ceglarska E, Kertesz VK, Lovei G, et al., Environmental risk
551 assessment for plant pests: A procedure to evaluate their impacts on ecosystem services. *Sci Total*
552 *Environ* 468: 475-486 (2014).
- 553 41. Ramoelo A, Skidmore AK, Cho MA, Schlerf M, Mathieu R and Heitkonig IMA, Regional estimation of
554 savanna grass nitrogen using the red-edge band of the spaceborne RapidEye sensor. *Int J Appl Earth*
555 *Obs* 19: 151-162 (2012).
- 556 42. Zheng Q, Huang WJ, Cui XM, Shi Y and Liu LY, New Spectral Index for Detecting Wheat Yellow Rust
557 Using Sentinel-2 Multispectral Imagery. *Sensors-Basel* 18(2018).
- 558

Table 1. The spectral characteristics of the Parrot Sequoia sensor.

Band	Central wavelength (nm)	Bandwidth(nm)
B1- Green	550	40
B2- Red	660	40
B3- Red-edge	735	10
B4-NIR	790	40

Table2. Random Forest model performance over features

Model	B1	B2	B3	B4	DSM	NDVI	RENDVI	OA	Kappa
Model1	-	-	-	-	-	-	+	0.8772	0.7611
Model2	-	-	-	-	-	+	+	0.9678	0.9471
Model3	-	+	-	-	-	+	+	0.9765	0.9544
Model4	-	+	-	+	-	+	+	0.9762	0.9536
Model5	-	+	-	+	+	+	+	0.9809	0.9630
Model6	+	+	-	+	+	+	+	0.9836	0.9683
Model7	+	+	+	+	+	+	+	0.9850	0.9709
Model8	+	+	+	+	-	-	-	0.9641	0.9408
Model9	+	+	+	+	+	-	-	0.9735	0.9514

Notes: "+" represents the added modeling features. "-" represents the removed modeling feature.

Table 3. Quantitative evaluation results different method

Method	MLP	NB	SVM	RF
Kappa	0.9196	0.9401	0.9424	0.9709
OA	0.9592	0.9637	0.9645	0.9850

Figures

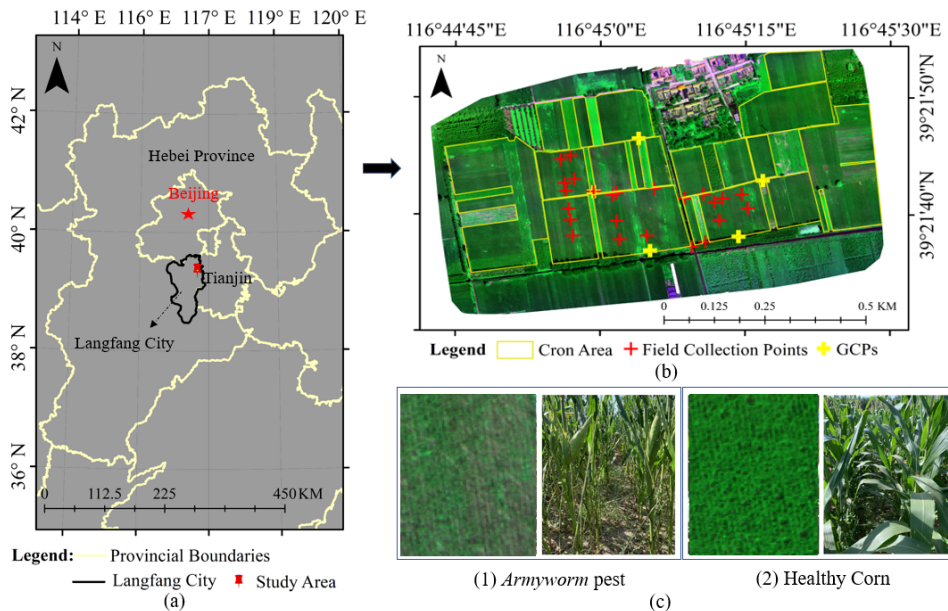
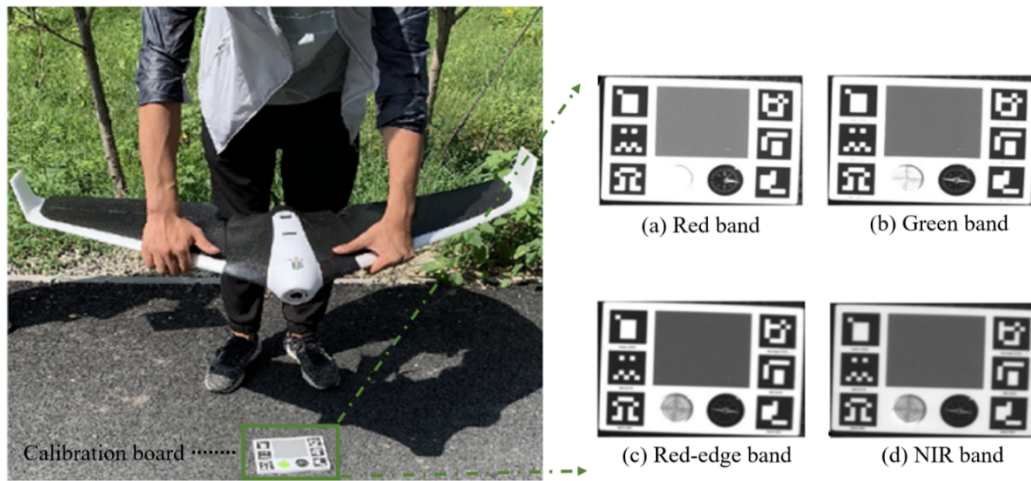


Figure 1. The location of study area (a). (b) UAV multispectral image (R (B2, red band)/G (B3, Red-edge band)/B (B1, green band)) and the spatial distribution of the field collection points and the GCPs. (c) The image pairs with UAV sub-image (R (B2, red band)/G (B3, Red-edge band)/B (B1, green band)) and corresponding photos taken in field campaign.

570



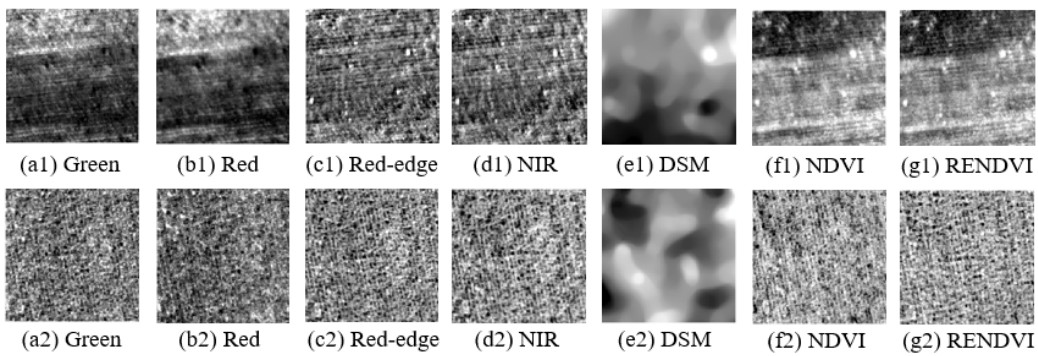
571

572

573

Figure 2. The fixed-wing UAV (left) and the captured images of calibration board with four spectral bands (right).

574



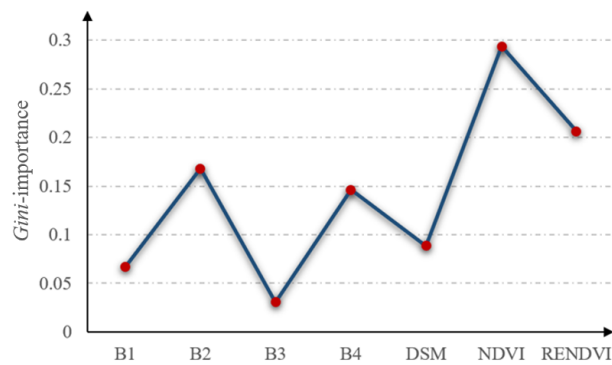
575

576

577

578

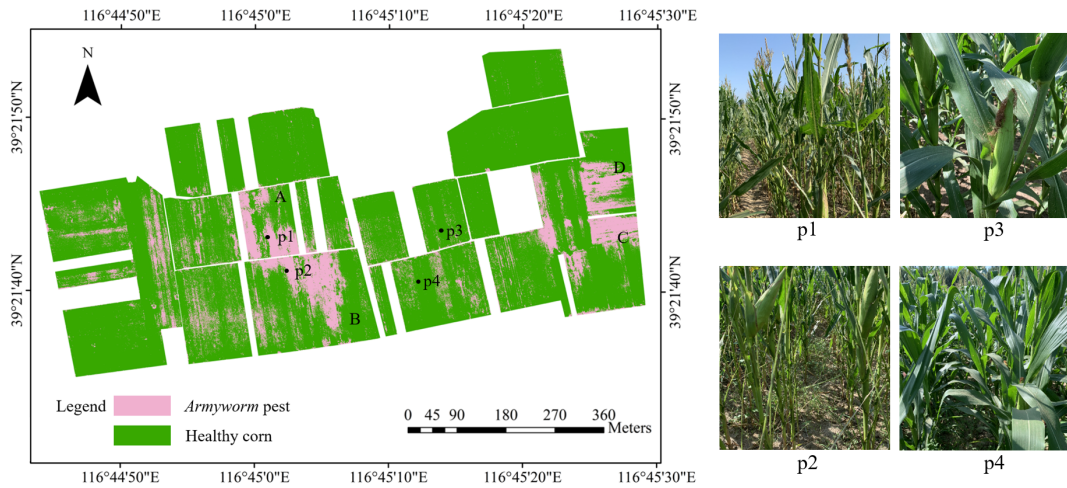
Figure 3. Visualization of image features for *armyworm* infested area (a1-g1) and healthy corn planted area (a2-g2).



579

580

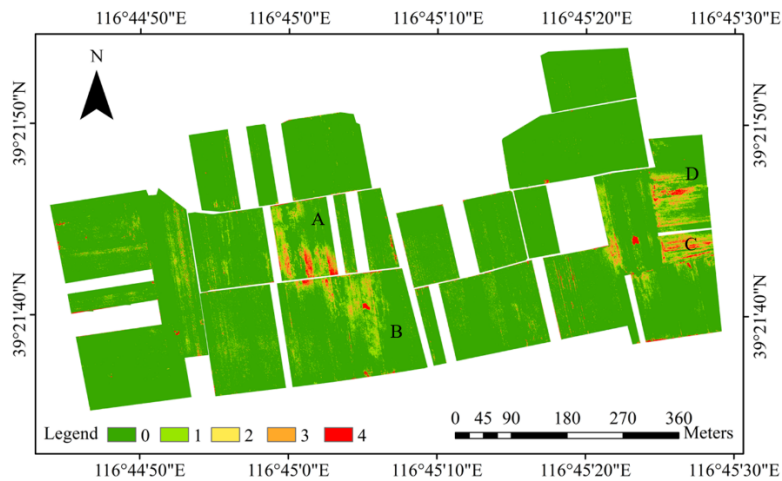
Figure 4. The *Gini*-importance of the image features.



581

582 **Figure 5.** Mapping result of corn planted area infested by *armyworm* pest by optimized RF model.
 583 The mark A, B, C and D are the investigated field plots with heavy *armyworm* pest. The photos of
 584 (p1) and (p2) are taken in the area infested by *armyworm*, and the photos of (p3) and (p4) are taken in
 585 the healthy corn planted area.

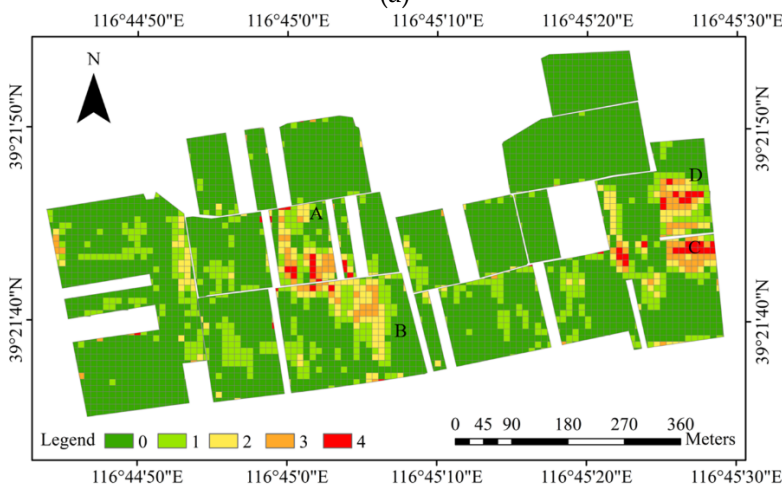
586



587

588

(a)



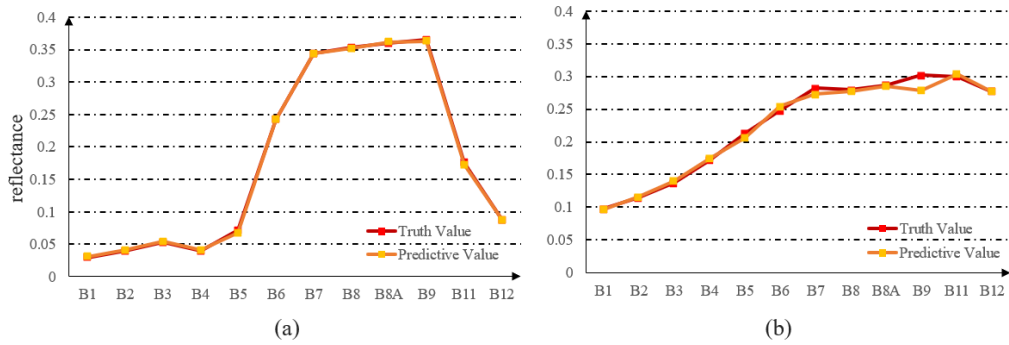
589

590

(b)

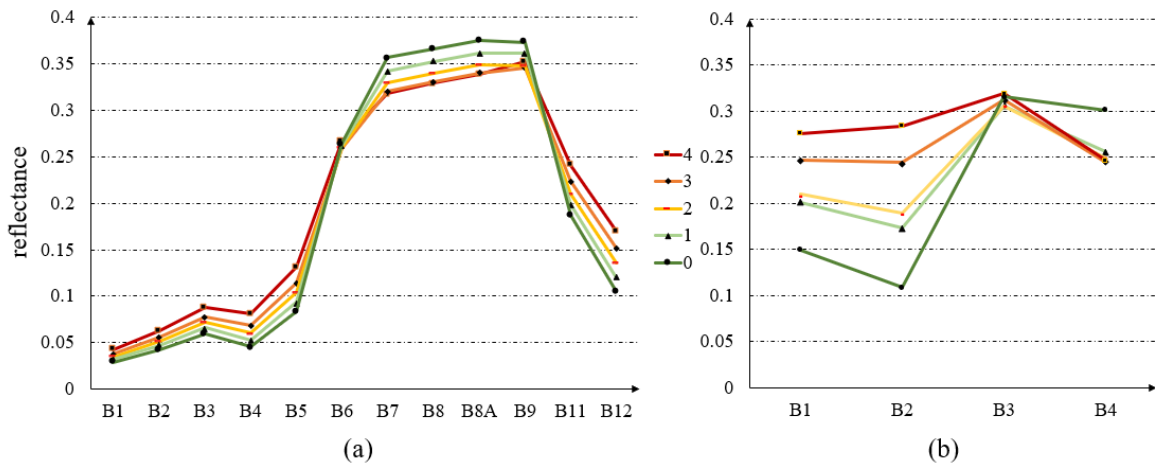
591 **Figure 6.** *Armyworm* pest incidence levels of corn planted area. (a) Infesting levels of insect pests
 592 based on UAV images. (b) Infesting levels resulting from (a) using statistical results of 10m × 10m

593 grid. The mark A, B, C and D are the investigated cornfield plots with serious *armyworm* pest
 594 infested area.
 595



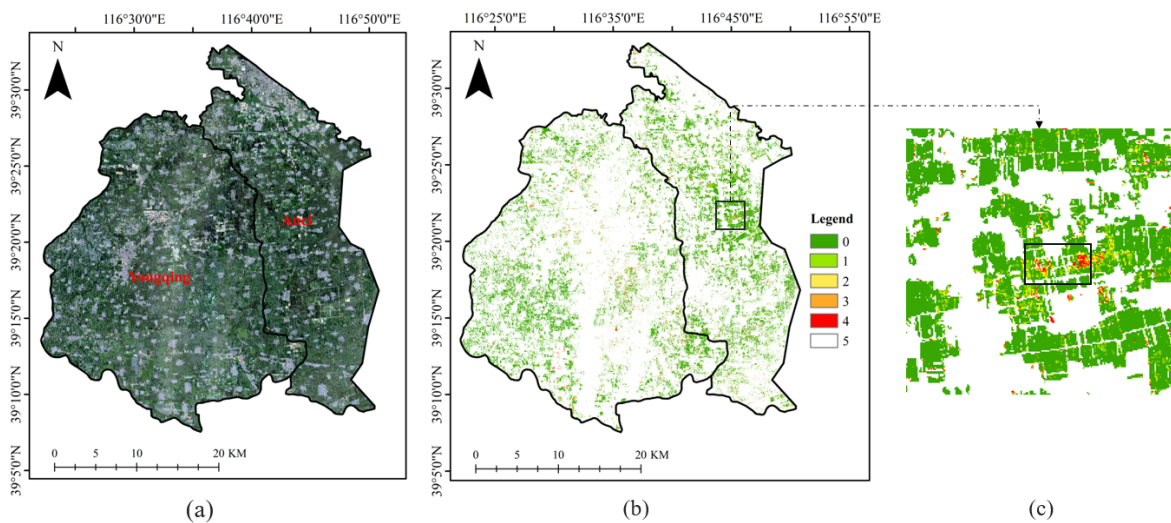
596
 597 **Figure 7.** Spectral changes of corn planted area (a) and buildings (b) before and after SupReME
 598 reconstruction.

599



600
 601 **Figure 8.** Spectral characteristics of different pest levels in Sentinel-2 image (a) and UAV image (b).

602



603
 604 **Figure 9.** Classification of armyworm pests based on Sentinel-2 image. (a) is sentinel-2 true color map. (b)
 605 Classification result of armyworm pest levels. (c) sub-image of (b).